J|A|C|S
ARTICLES
Published on Web 11/26/2003

Systematic Synthesis and Characterization of Single-Crystal Lanthanide Orthophosphate Nanowires

Yue-Ping Fang,[†] An-Wu Xu,*[,†] Rui-Qi Song,[†] Hua-Xin Zhang,[†] Li-Ping You,[§] Jimmy C. Yu,[‡] and Han-Qin Liu[†]

Contribution from the School of Chemistry and Chemical Engineering, Zhongshan University, Guangzhou, 510275, China; Department of Chemistry, The Chinese University of Hong Kong, Shatin, New Territories, Hong Kong, China; and Electron Microscopy Laboratory, Peking University, Beijing, 100084, China

Received July 15, 2003; E-mail: cedc17@zsu.edu.cn

Abstract: A simple hydrothermal method has been developed for the systematic synthesis of lanthanide orthophosphate crystals with different crystalline phases and morphologies. It has been shown that pure $LnPO_4$ compounds change structure with decreasing Ln ionic radius: i.e., the orthophosphates from Ho to Lu as well as Y exist only in the tetragonal zircon (xenotime) structure, while the orthophosphates from La to Dy exist in the hexagonal structure under hydrothermal treatment. The obtained hexagonal structured lanthanide orthophosphate $LnPO_4$ (Ln = La, Ce, Pr, Nd, Sm, Eu, Gd, Tb, and Dy) products have a wirelike morphology. In contrast, tetragonal $LnPO_4$ (Ln = Ho, Er, Tm, Yb, Lu, Y) samples prepared under the same experimental conditions consist of nanoparticles. The obtained hexagonal $LnPO_4$ (Ln = La → Tb) can convert to the monoclinic monazite structured products, and their morphologies remained the same after calcination at 900 °C in air (Hexagonal $DyPO_4$ is an exceptional case, it transformed to tetragonal $DyPO_4$ by calcination), while the tetragonal structure for (Ho→ Lu, Y)PO_4 remains unchanged by calcination. The resulting $LnPO_4$ (Ln = La → Dy) products consist almost entirely of nanowires/nanorods with diameters of 5−120 nm and lengths ranging from several hundreds of nanometers to several micrometers. Europium doped $LaPO_4$ nanowires were also prepared, and their photoluminescent properties were reported. The optical absorption spectrum of $CePO_4$ nanowires was measured and showed some differences from that of bulk $CePO_4$ materials. The possible growth mechanism of lanthanide phosphate nanowires was explored in detail. X-ray diffraction, field-emission scanning electron microscopy, transmission electron microscopy, electron diffraction, infrared absorption spectra, X-ray photoelectron spectroscopy, optical absorption spectra, and photoluminescence spectra have been employed to characterize these materials.

Introduction

Dimensionality plays an important role in determining the properties of nanomaterials and in the synthesis of nanostructured materials with controlled morphology, size, chemical composition, and crystal structure.[1−3] Due to the discovery of carbon nanotubes, a lot of one-dimensional (1D) nanomaterials have been extensively investigated during the past few decades because of their potential technological applications.[4−7] Aside from nanotubes,[8−10] a variety of 1D nanowires including oxides,[11] metal and alloys,[12] semiconductors,[14] metal chalcogenides,[13] and polymers,[15] and so forth have been synthesized

[†] Zhongshan University.
[‡] The Chinese University of Hong Kong.
[§] Peking University.

(1) Hu, J.; Odom, W.; Lieber, C. M. *Acc. Chem. Res.* **1999**, *32*, 435.
(2) Kovtyukhova, N. I.; Mallouk, T. E. *Chem.—Eur. J.* **2002**, *8*, 4355.
(3) Xia, Y.; Yang, P.; Sun, Y,; Wu, Y.; Mayers, B.; Gates, B.; Yin, Y.; Kim, F.; Yan, H. *Adv. Mater.* **2003**, *15*, 353 and references therein.
(4) Wu, Y.; Yan, H.; Huang, M.; Messer, B.; Song, J. H.; Yang, P. *Chem.—Eur. J.* **2002**, *8*, 1261.
(5) (a) Feldman, Y.; Wasserman, E.; Srolovita, D. J.; Tenne, R. *Science* **1995**, *267*, 222. (b) Brorson, M.; Hansen, T. W.; Jacobsen, C. J. H. *J. Am. Chem. Soc.* **2002**, *124*, 11582. (c) Rao, C. N. R.; Satishkumar, B. C.; Govindaraj, A.; Nath, M. *ChemPhysChem* **2001**, *2*, 78. (d) Tenne, R. *Chem.—Eur. J.* **2002**, *8*, 5297. (f) Remskar, M.; Mrzel, A.; Skraba, Z.; Jesih, A.; Ceh, M.; Demšar, J.; Stadelmann, P.; Lévy, F.; Mihailovic, D. *Science* **2001**, *292*, 479.
(6) Yan, H.; He, R.; Johnson, J.; Law, M.; Saykally, R.; Yang, P. *J. Am. Chem. Soc.* **2003**, *125*, 4728.
(7) Pan, Z. W.; Dai, Z. R.; Wang, Z. L. *Science* **2001**, *291*, 1947.
(8) Iijima, S. *Nature* **1991**, *354*, 56.
(9) (a) Xu, A. W.; Fang, Y. P.; You, L. P.; Liu, H. Q. *J. Am. Chem. Soc.* **2003**, *125*, 1494. (b) Yada, M.; Mihara, M.; Mouri, S.; Kuroki, M.; Kijima, T. *Adv. Mater.* **2002**, *14*, 309.
(10) Goldberger, J.; He, R.; Zhang, Y.; Lee, S.; Yan, H.; Choi, H. J.; Yang, P. *Nature* **2003**, *422*, 599.
(11) (a) Dai, Z. R.; Gole, J. L.; Stout, J. D.; Wang, Z. L. *J. Phys. Chem. B* **2002**, *106*, 1274. (b) Zhang, D.; Sun, L.; Yin, J.; Yan, C. *Adv. Mater.* **2003**, *15*, 1022. (c) Dai, Z. R.; Pan, Z. W.; Wang, Z. L. *J. Phys. Chem. B* **2002**, *106*, 902. (d) Wang, W.; Xu, C.; Wang, G.; Liu, Y.; Zheng, C. *Adv. Mater.* **2002**, *14*, 837. (e) Yang, P.; Lieber, C. M. *J. Mater. Res.* **1997**, *12*, 2981.
(12) (a) Zhang, Z.; Blom, D. A.; Gai, Z.; Thompson, J. R.; Shen, J.; Dai, S. *J. Am. Chem. Soc.* **2003**, *125*, 7528. (b) Sun, Y.; Gates, B.; Mayers, B.; Xia, Y. *Nano Lett.* **2002**, *2*, 165. (c) Murphy, C. J.; Jana, N. R. *Adv. Mater.* **2002**, *14*, 80.
(13) (a) Duan, X.; Lieber, C. M. *Adv. Mater.* **2000**, *12*, 298. (b) Duan, X.; Huang, Y.; Cui, Y.; Wang, J.; Lieber, C. M. *Nature* **2001**, *409*, 66. (c) Hanrath, T.; Korgel, B. A. *J. Am. Chem. Soc.* **2002**, *124*, 1424. (d) Ma, D. D. D.; Lee, C. S.; Au, F. C. K.; Tong, S. Y.; Lee, S. T. *Science* **2003**, *299*, 1874.
(14) (a) Geng, B.; Wang, G.; Jiang, A.; Xie, T.; Sun, S.; Meng, G.; Zhang, L. *Appl. Phys. Lett.* **2003**, *82*, 4791. (b) Yang, C.; Awschalom, D. D.; Stucky, G. D. *Chem. Mater.* **2002**, *14*, 1277. (c) Sone, E. D.; Zubarev, E. R.; Stupp, S. I. *Angew. Chem., Int. Ed.* **2002**, *41*, 1706.
(15) (a) Gao, M.; Huang, S.; Dai, L.; Wallace, G.; Gao, R.; Wang, Z. *Angew. Chem., Int. Ed.* **2000**, *39*, 3664. (b) Fu, M.; Zhu, Y.; Tan, R.; Shi, G. *Adv. Mater.* **2001**, *13*, 1874.

and their novel properties have also been extensively explored. These 1D nanostructured materials have been shown to play an important role as active components or interconnects in fabricating nanoscale electronic, optical, optoelectronic, electrochemical, and electromechanical devices.[16] Notable examples of demonstrated applications include field-effect transistors (FETs),[17] light-emitting diodes (LEDs),[13b] single-electron transistors,[18] biological and chemical sensors,[19] photodetectors,[20] electron emitters,[21] and ultraviolet lasers.[6]

Although a number of synthetic methodologies have been developed to fabricate and assemble 1D nanostructures,[22] they often suffer from the requirements of high temperature, special conditions, tedious procedures, and catalysts or templates. Therefore, the development of practical methods for fabricating large numbers of 1D nanostructures at low cost is still a great challenge for future study. Chemical methods, on the other hand, seem to provide an alternative and intriguing strategy for generating 1D nanostructures with respect to material diversity, cost, versatility, synthetic tunability, and potential for large-volume production. Of the methods employed in the synthesis of 1D nanomaterials, hydrothermal methods have been regarded as effective routes to the fabrication of high-quality anisotropic nanomaterials.[23] Several solution-phase procedures have been demonstrated for generating 1D nanostructures.[24] More recently, some studies have been reported on the synthesis of lanthanide hydroxide nanotubes and nanowires/nanorods by hydrothermal processes.[25] Conventionally, bulk monazite-type (high-temperature phase) lanthanide phosphates have been prepared by solid-phase reaction at high temperature.[26] $LnPO_4$ and rare earth ion doped $LnPO_4$ nanoparticles or colloids have also been prepared by solution precipitation methods, and their photoluminescence properties have been studied.[27] However, previously there have been no systematic accounts of synthesis, characterization, and properties of $LnPO_4$ nanowires and the correlation between $LnPO_4$ morphologies with the crystal structures. These details will be presented in this article, where we report a systematic synthesis and characterization of high-quality $LnPO_4$ and lanthanide ion doped $LnPO_4$ single-crystal nanowires with controlled crystal phases obtained by hydrothermal treatment. The measurements of the photoluminescence emission and photoluminescence excitation spectra of rare earth activated $LnPO_4$ nanowires/nanorods were performed. The growth mechanism of $LnPO_4$ nanowires is also discussed based on the inherent crystal structure of these materials.

Orthophosphates are substances that are composed of isolated PO_4 tetrahedra, analogous to "orthosilicates". The most common naturally occurring orthophosphates are apatite $[Ca_5(PO_4)_3(F,Cl,OH)]$ and monazite ($LnPO_4$), where Ln refers to lanthanide elements. Lanthanide phosphates have several polymorphic forms. They appear in hexagonal, tetragonal, and monoclinic modifications. The hexagonal structure is the low-temperature phase, and it can transform into the monoclinic structure, while the tetragonal maintains its structure after calcination at 900 °C.[28−31] Lanthanide compounds have been extensively used as high performance luminescent devices, magnets, catalysts, time-resolved fluorescence labels for biological detection, and other functional materials based on the electronic, optical, and chemical characteristics resulting from the 4f shell of their ions.[32] Lanthanide orthophosphates ($LnPO_4$) have a variety of potentially beneficial properties, including very low solubility in water (their solubility products are on the level of 10^{-25} to 10^{-27}),[33] high thermal stability (the melting points of $LnPO_4$ are around 2300 °C),[34] high index of refraction, and, in the cases of Nd, Eu, etc., high concentrations of lasing ions.[35] These properties provide the basis for interest in their use in a wide range of applications such as phosphors, sensors, proton conductors, ceramic materials, catalysts, and heat-resistant materials.[36,37] Very recently, lanthanide phosphates have been of interest for use as inert matrixes for Pu fuel and as multilayered (with Al_2O_3 and ZrO_2) weak-bonded ceramic composites.[38] They also have

(16) (a) Huang, Y.; Duan, X.; Wei, Q.; Lieber, C. M. *Science* **2001**, *291*, 630. (b) Huang, M. H.; Mao, S.; Feick, H.; Yan, H.; Wu, Y.; Kind, H.; Weber, E.; Russo, R.; Yang, P. *Science* **2001**, *292*, 1897. (c) Wang, Z. L. *Adv. Mater.* **2000**, *12*, 1295. (d) Dekker, C. *Phys. Today* **1999**, *May* 22. (e) Frank, S.; Poncharal, P.; Wang, Z. L.; de Heer, W. A. *Science* **1998**, *280*, 1744.

(17) (a) Chung, S. W.; Yu, J. Y.; Heath, J. R. *Appl. Phys. Lett.* **2000**, *76*, 2068. (b) Tans, J. S.; Verschueren, R. M.; Dekker, C. *Nature* **1998**, *393*, 49.

(18) (a) Tans, S. J.; Devoret, M. H.; Dal, H.; Thess, A.; Smalley, R. E.; Gerrligs, L. J. Dekker, C. *Nature* **1997**, *386*, 474. (b) Bockrath, M.; Cobden, D. H.; McEuen, P. L.; Chopra, N. G.; Zettl, A.; Thess, A.; Smalley, R. E.; *Science* **1997**, *275*, 1922.

(19) (a) Cui, Y.; Wei, Q.; Park, H.; Lieber, C. M. *Science* **2001**, *293*, 1289. (b) Nicewarner-Peña, S. R.; Freeman, R. G.; Reiss, B. D.; He, L.; Peña, D. J.; Walton, I. D.; Cromer, R.; Keating C. D.; Natan, M. J. *Science* **2001**, *294*, 137.

(20) Wang, J.; Gudiksen, M. S.; Duan, X.; Cui, Y.; Lieber, C. M. *Science* **2001**, *293*, 1455.

(21) Davydov, D. N.; Sattari, P. A.; AlMawlawi, D.; Osika, A.; Haslett, T. L.; Moskovits, M. *J. Appl. Phys.* **1999**, *86*, 3983.

(22) (a) Wu, Y.; Yan, H.; Huang, M.; Messer, B.; Song, J. H.; Yang, P. *Chem.—Eur. J.* **2002**, *8*, 1261. (b) Zhu, H.; Xu, C.; Wu, D.; Wei, B.; Vajtai, R.; Ajayan, P. M. *Science* **2002**, *296*, 884. (c) Brorson, M.; Hansen, T. W.; Jacobsen, C. J. H. *J. Am. Chem. Soc.* **2002**, *124*, 11582. (d) Ajayan, P. M.; Stephan, O.; Redlich, P.; Colliex, C. *Nature* **1995**, *375*, 564. (e) Han, W.; Fan, S.; Li, Q.; Hu, Y. *Science* **1997**, *277*, 1287. (f) Routkevitch, D.; Bigioni, T.; Moskovits, M.; Xu, J. M. *J. Phys. Chem.* **1996**, *100*, 14037.

(23) Patzke, G. R.; Krumeich, F.; Nesper, R. *Angew. Chem., Int. Ed.* **2002**, *41*, 2446.

(24) (a) Niederberger, M.; Muhr, H.-J.; Krumeich, F.; Bieri, F.; Günther, D.; Nesper, R. *Chem. Mater.* **2000**, *12*, 1995. (b) Kuang, D. B.; Xu, A. W.; Fang, Y. P.; Ou, H. D.; Liu, H. Q. *J. Cryst. Growth* **2002**, *244*, 379. (c) Vayssieres, L. *Adv. Mater.* **2003**, *15*, 464. (d) Holmes, J. D.; Johnston, K. P.; Doty, R. C.; Korgel, B. A. *Science*, **2000**, *287*, 1471.

(25) (a) Xu, A. W.; Fang, Y. P.; You, L. P.; Liu, H. Q. *J. Am. Chem. Soc.* **2003**, *125*, 1494. (b) Wang, X.; Li, Y. D. *Angew. Chem., Int. Ed.* **2002**, *41*, 4790.

(26) (a) Kizilyalli, M.; Welch, A. J. E. *J. Appl. Crystallogr.* **1976**, *9*, 413. (b) Mullica, D. F.; Milligan, W. O.; Grossie, D. A. Beall, G. W.; Boatner, L. A. *Inorg. Chim. Acta* **1984**, *95*, 231. (c) Wang, R.; Pan, W.; Chen, J.; Fang, M.; Cao, Z.; Luo, Y. *Mater. Chem. Phys.* **2003**, *79*, 30.

(27) (a) Riwotzki, K.; Meyssamy, H.; Schnablegger, H.; Kornowski, A.; Haase, M. *Angew. Chem., Int. Ed.* **2001**, *40*, 573. (b) Haase, M.; Riwotzki, K.; Meyssamy, H.; Kornowski, A. *J. Alloys Compd.* **2000**, *303−304*, 191. (c) Heer, S.; Lehmann, O.; Haase, M.; GÜdel, H. U. *Angew. Chem., Int. Ed.* **2003**, *42*, 3179. (d) Riwotzki, K.; Meyssamy, H.; Kornowski, A.; Haase, M. *J. Phys. Chem.* B **2000**, *104*, 2824. (e) Kijkowska, R. *J. Mater. Sci.* **2003**, *38*, 229.

(28) Hezel, A.; Ross, S. D. *J. Inorg. Nucl. Chem.* **1967**, *29*, 2085.

(29) Meldrum, A.; Boatner, L. A.; Ewing, R. C. *Phys. Rev. B* **1997**, *56*, 13805.

(30) Kijkowska, R.; Cholewka, E.; Duszak, B. *J. Mater. Sci.* **2003**, *38*, 223.

(31) (a) Li, B.; Shen, L.; Liu, X.; Wang, T.; Ishii, K.; Sakaki, Y.; Kashiwaya, Y.; Takahashi, H.; Shibayama, T. *J. Mater. Sci. Lett.* **2000**, *19*, 343. (b) Onoda, H.; Nariai, H.; Maki, H.; Motooka, I. *Mater. Chem. Phys.* **2002**, *73*, 19.

(32) (a) Adachi, G. Y.; Imanaka, N. *Chem. Rev.* **1998**, *98*, 1479. (b) Xu, A. W.; Gao, Y.; Liu, H. Q. *J. Catal.* **2002**, *207*, 151. (c) Peruski, A. H.; Johnson, L. H.; Peruski, L. F. *J. Immunol. Methods* **2002**, *263*, 35−41. (d) Capobianco, J. A.; Boyer, J. C.; Vetrone, F.; Speghini, A.; Bettinelli, M. *Chem. Mater.* **2002**, *14*, 2915. (e) Dhanaraj, J.; Jagannathan, R.; Kutty, T. R. N.; Lu, C. H. *J. Phys. Chem. B* **2001**, *105*, 11098.

(33) Firsching, F. H.; Brune, S. N. *J. Chem. Eng. Data* **1991**, *36*, 93.

(34) Rouanel, A.; Serra, J. J.; Allaf, K.; Orlovskii, V. P. *Inorg. Mater.* **1981**, *17*, 76.

(35) Guo, Y.; Woznicki, P.; Barkatt, A.; Saad, E. E.; Talmy, I. G. *J. Mater. Res.* **1996**, *11*, 639.

(36) (a) Nishihama, S.; Hirai, T.; Komasawa, I. *J. Mater. Chem.* **2002**, *12*, 1053. (b) Onoda, H.; Nariai, H.; Moriwaki, A.; Maki, H.; Motooka, I. *J. Mater. Chem.* **2002**, *12*, 1754.

(37) Ordonez-Regil, E.; Drot, R.; Simoni, E.; Ehrhardt, J. J. *Langmuir* **2002**, *18*, 7977.

(38) (a) Uskakov, S. V.; Helean, K. B.; Navrotsky, A.; Boatner, L. A. *J. Mater. Res.* **2001**, *16*, 2623. (b) Matzke, Hj.; Rondinella, V. V.; Wiss, T. *J. Nucl. Mater.* **1999**, *274*, 47. (c) Kleykamp, H. *J. Nucl. Mater.* **1999**, *275*, 1. (d) Marshall, D. B.; Morgan, P. E.; Housley, R. M. *J. Am. Ceram. Soc.* **1997**, *80*, 1677. (e) Mawdsley, J. R.; Kovar, D.; Halloran, J. W. *J. Am. Ceram. Soc.* **2000**, *83*, 802.

properties that make them of interest as scintillators for X-ray and γ-ray detection in medical imaging applications, as thermophosphors for remote temperature measurements, and as hosts for microlasers.[39] Recently, ceramic $LaPO_4$ doped with 1−5 mol % Sr has been found to exhibit proton conduction in a wet atmosphere at high temperature. Such solid-state protonic conductors are candidates as electrolytes in fuel cells, hydrogen separation membranes, and sensors.[40] Lanthanide phosphates have been shown to be a useful host lattice for lanthanide ions to produce phosphors emitting a variety of colors.[27,41] Ce^{3+} and Tb^{3+} coactivated bulk $LaPO_4$ is a highly efficient and commercially applied green ($^5D_4-^7F_5$ of Tb^{3+} at 543 nm) phosphor in fluorescent lamps.[27a,42] In compact lamps, the wall temperature is in the range of 150−200 °C. At these temperatures, most lamp phosphors degrade, but $LaPO_4$/Ce/Tb phosphor is stable at high temperatures.[42] Nanoscaled phosphors could have some potential advantages over conventional micron-sized phosphors.[43] The properties of lanthanide compounds depend strongly on the compositions and structure, which are sensitive to the bonding states of lanthanide ions. If lanthanide compounds were fabricated in the form of a 1D nanostructure (e.g., nanowires) with a different crystal structure, they would have new functionalities as a result of their marked specific shape. They would also act as electrically, magnetically, or optically functional host materials for rare earth ions in phosphor displays, waveguide devices, fluorescence labels for biological detection, and the active material in lasers.[44]

Experimental Section

Preparation. Hexagonal (La → Dy)PO_4 nanowires (or nanorods) and tetragonal (Ho → Lu, Y)PO_4 nanoparticles were prepared by a simple hydrothermal method. In a typical synthesis, 10 mL of $NH_4H_2PO_4$ (0.4 M) aqueous solution were added into 10 mL of $Ln(NO_3)_3$ (Ln = La, Ce, Pr, Nd, Sm, Eu, Gd, Tb, Dy, Ho, Er, Tm, Yb, Lu, and nonlanthanide Y) aqueous solution (0.4 M) under vigorous stirring for 20 min. The pH was adjusted to a specific value using aqueous ammonia (27 wt %) solution. The resulting suspension was poured into a Teflon-lined stainless steel autoclave. The autoclave was sealed and maintained at 150 °C for 12 h and then air cooled to room temperature. The resulting $LnPO_4$ products were filtered, washed with deionized water and absolute alcohol to remove ions possibly remaining in the final products, and finally dried at 80 °C in air for further characterization. $LaPO_4$ nanowires doped with 5 mol % europium were prepared according to the same method. To prepare $CePO_4$ nanowires, the suspension in the autoclave was first purged with argon for 60 min to prevent oxidation of Ce^{3+} to Ce^{4+} before heating. Monoclinic (La → Tb)PO_4 and tetragonal $DyPO_4$ nanowires/nanorods were prepared by calcination of hydrothermally obtained corresponding products at 900 °C in air.

Characterization. The X-ray powder diffraction (XRD) patterns of all samples were performed on a Rigaku/Max-3A X-ray diffractometer with Cu Kα radiation ($\lambda = 1.5418$ Å). The operation voltage and current were maintained at 40 kV and 40 mA, respectively. Field-emission scanning electron microscopic (FE-SEM) images were obtained with a JEOL JSM-6330F operated at a beam energy of 10.0 kV. Transmission electron microscopic (TEM) images, high-resolution transmission electron microscopic (HRTEM) images, and the selected area electron diffraction (SAED) patterns were obtained on a JEOL-2010 microscope with an accelerating voltage of 200 kV. Energy-dispersive X-ray spectroscopy (EDS) was attached to the JEOL 2010. Sample grids were prepared by sonicating powdered samples in ethanol for 20 min and evaporating one drop of the suspension onto a carbon-coated, holey film supported on a copper grid for TEM measurements. A Shimadzu spectrophotometer (model 2501 PC) equipped with an integrating sphere was used to record the UV−vis diffuse reflectance spectra of the samples. The excitation and emission spectra were recorded with an F-4500 spectrophotometer equipped with a 150 W xenon lamp as the excitation source. All the measurements were performed at room temperature. Fourier transform infrared spectroscopy (FTIR) analysis was carried out using KBr disks in the region of 4000−400 cm^{-1} by using FTIR-Bruker-EQUINOX-55 at ambient conditions. X-ray photoelectron spectroscopy (XPS) measurements were performed in a VG Scientific ESCALAB Mark II spectrometer equipped with two ultra-high-vacuum (UHV) chambers. All binding energies were referenced to the C1s peak at 284.8 eV of the surface adventitious carbon.

Results and Discussion

I. Synthsis and Characterization of Hexagonal (La → Dy)-PO_4 Nanowires and Tetragonal (Ho → Lu, Y)PO_4 Crystals. Under identical synthetic conditions (at 150 °C for 12 h, pH 1−2), two different types of crystal structure of the obtained $LnPO_4$ products have been identified by X-ray diffraction (XRD) analyses. XRD patterns of the obtained hexagonal $LnPO_4$ (Ln = La, Ce, Pr, Nd, Sm, Eu, Gd, Tb, Dy) nanowires/nanorods and tetragonal (Ho → Lu, Y)PO_4 nanoparticles are shown in Figures S1 and S2 (Supporting Information), respectively. All the peaks of the XRD patterns for each sample in Figure S1 can be readily indexed to a pure hexagonal phase [space group: $P3_121$ (152)] of (La → Dy)PO_4, in good agreement with the data in the JCPDS cards. XRD results show that all nine $LnPO_4$ (Ln = La → Dy) crystals are isostructural. Moreover, the intensity of the (200) peak is much stronger than those of the other peaks, which is different from bulk hexagonal $LnPO_4$ (Ln = La → Dy).[30] This indicates that the obtained $LnPO_4$ (Ln = La → Dy) nanowires/nanorods grow preferentially along the [001] direction (the *c* axis). This is further demonstrated below by HRTEM and ED measurements. All diffraction peaks shown in Figure S2 are characteristic of a pure tetragonal phase [space group: $I4_1/amd$ (141)] of (Ho → Lu, Y)PO_4 (the nonlanthanide YPO_4 also has a tetragonal structure, so it is included in the present study). It is can be seen that six (Ho → Lu, Y)PO_4 samples are isostructural. Moreover, XRD analyses show systematic shifts in the positions of the diffraction peaks reflecting the contraction of the ionic radii of the lanthanides, as clearly seen from Figures S1 and S2. The unit cell dimensions of all $LnPO_4$ crystals calculated from XRD patterns are consistent with those reported in the JCPDS cards.

The measured lattice parameters *a* and *c*, plotted against the revised crystal (CR) ionic radii of the eight-coordinated trivalent lanthanide cations,[45] are presented in Figure 1. The

(39) (a) Moses, W. W.; Weber, M. J.; Derezno, S. E.; Perry, D.; Berdahl, P.; Boatner, L. A. *IEEE Trans. Nucl. Sci.* **1998**, *45*, 462. (b) Allison, S. W.; Boatner, L. A.; Gillies, G. T. *Appl. Opt.* **1995**, *25*, 5624. (c) Rapaport, A.; David, V.; Bass, M.; Deka, C.; Boatner, L. A. *J. Lumin.* **1999**, *85*, 155.
(40) (a) Norby, T.; Christiansen, N. *Solid State Ionics* **1995**, *77*, 240. (b) Amezawa, K.; Maekawa, H.; Tomii, Y.; Yamamoto, N. *Solid State Ionics* **2001**, *145*, 233. (c) Tyholdt, F.; Horst, J. A.; Jørgensen, S.; Østvold, T.; Norby, T. *Surf. Interface Anal.* **2000**, *30*, 95.
(41) (a) Dexpert-Ghys, J.; Mauricot, R.; Faucher, M. D. *J. Lumin.* **1996**, *69*, 203. (b) Rambabu, U.; Munirathnam, N. R.; Prakash, T. L.; Buddhudu, S. *Mater. Chem. Phys.* **2002**, *78*, 160. (c) Wu, X.; You, H.; Cui, H.; Zeng, X.; Hong, G.; Kim, C. H.; Pyun, C. H.; Yu, B. Y.; Park, C. H. *Mater. Res. Bull.* **2002**, *37*, 1531.
(42) (a) Kang, Y.; Kim, E. J.; Lee, D. Y.; Park, H. D. *J. Alloys Compd.* **2002**, *347*, 266. (b) Lenggoro, I. W.; Xia, B.; Mizushima, H.; Okuyama, K.; Kijima, N. *Mater. Lett.* **2001**, *50*, 92.
(43) (a) Bhargava, R. N.; Gallagher, D.; Hong, X.; Nurmikko, A. *Phys. Rev. Lett.* **1994**, *72*, 416. (b) Holmes, J. D.; Ziegler, K. J.; Doty, R. C.; Pell, L. E.; Johnston, K. P.; Korgel, B. A. *J. Am. Chem. Soc.* **2001**, *123*, 3743.
(44) (a) Schuetz, P.; Caruso, F. *Chem. Mater.* **2002**, *14*, 4509. (b)
(45) Shannon, R. D. *Acta Crystallogr. A* **1976**, *32*, 751.

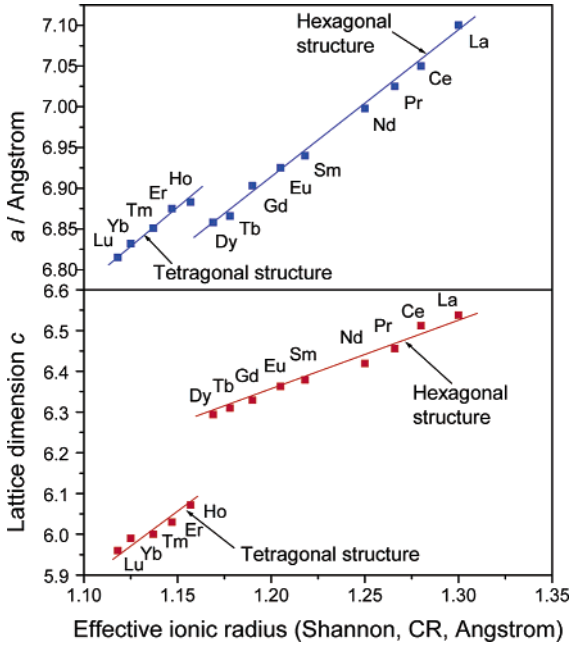

Figure 1. Plots of the measured lattice constants *a* (top) and *c* (bottom) of the obtained hexagonal and tetragonal $LnPO_4$ against lanthanide ionic radius.

approximately linear plots show the expected effect of the lanthanide contraction. On the other hand, it is clearly observed from Figure 1 that La, Ce, Pr, Nd, Sm, Eu, Gd, Tb, and Dy are located at one line and that their phosphates have a hexagonal structure, while Ho, Er, Tm, Yb, and Lu are located on the other line and their phosphates have a tetragonal structure. Why does $LnPO_4$ (Ln = La → Dy) have a hexagonal structure and (Ho → Lu, Y)PO_4 crystallize in a tetragonal structure under the same synthetic conditions? It is believed that this could be associated with the change of lanthanide ion radius, although the exact reason is not clear at present. In fact, the same phenomena have also been observed for $LnPO_4$ crystals prepared directly by solid-phase reaction at high temperature (900−1300 °C). It is found that $LnPO_4$ (Ln = La → Dy) crystallize in the monoclinic form, while (Ho → Lu, Y)PO_4 exist in the tetragonal structure under direct solid-phase reaction conditions. Obviously, the monoclinic is a high-temperature phase, and the hexagonal is a low-temperature phase; the structure transition from the hexagonal to the monoclinic can be observed by calcination at high temperature. This will be further demonstrated below.

The morphology of the samples was examined with scanning electron microscopy (SEM) and transmission electron microscopy (TEM). SEM images of the obtained $PrPO_4$, $SmPO_4$, $GdPO_4$, $TbPO_4$, and $DyPO_4$ nanowires/nanorods are shown in Figures 2a, b, c, d, and S3e, respectively, and shown in Figure 3a, b, S3c, and S3d (Figure S3, Supporting Information) are the TEM images of the obtained $LaPO_4$, $CePO_4$, $NdPO_4$, and $EuPO_4$ nanowires/nanorods, respectively. The as-synthesized $LnPO_4$ (Ln = La → Dy) products consist almost entirely of nanowires/nanorods with diameters of 5−120 nm and lengths ranging from several hundreds of nanometers to several micrometers. The high density of nanowires is representative of the high yields (close to 100%) associated with this new preparation approach. The results demonstrate that high-quality hexagonal structured $LnPO_4$ (Ln = La → Dy) nanowires/nanorods can be obtained by this simple method. It is worth noting that $DyPO_4$ nanowires aggregate into large bundles, as clearly shown in Figure S3e (Figure S3, Supporting Information).

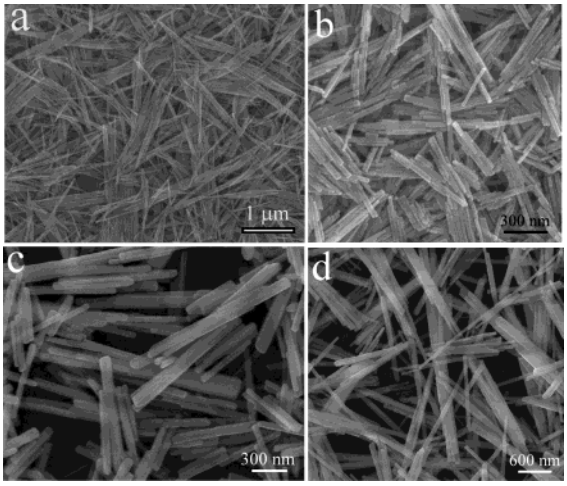

Figure 2. SEM images of the as-synthesized $LnPO_4$ nanowires by hydrothermal treatment. (a) $PrPO_4$, (b) $SmPO_4$, (c) $GdPO_4$, (d) $TbPO_4$.

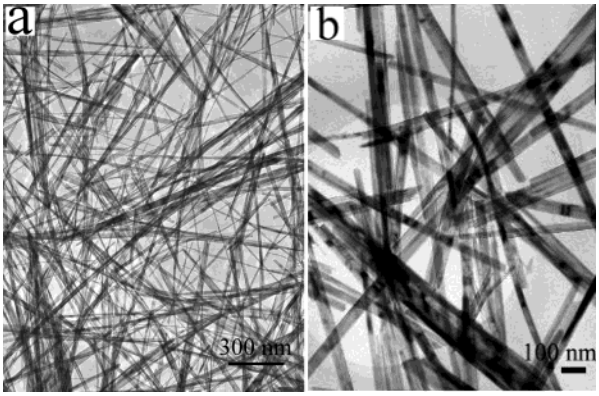

Figure 3. TEM images of the obtained hexagonal $LaPO_4$ (a) and $CePO_4$ (b) nanowires or nanorods.

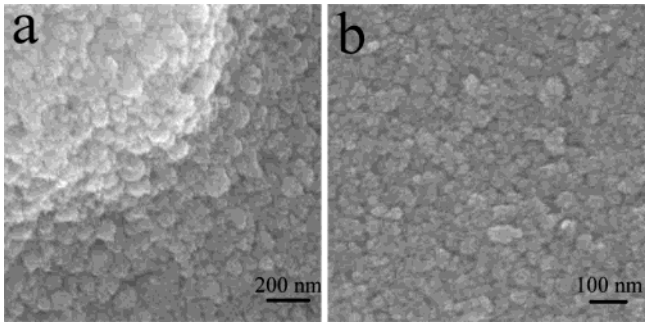

Figure 4. SEM images of the obtained tetragonal $ErPO_4$ (a) and $LuPO_4$ (b) nanoparticles.

Under the same synthetic conditions, (Ho → Lu, Y)PO_4 crystals with particle morphology can be observed. Figure 4a and b shows SEM images of the obtained tetragonal structured $ErPO_4$ and $LuPO_4$ crystals, respectively. YPO_4, $HoPO_4$, $TmPO_4$, and $YbPO_4$ can also be obtained only in the form of irregularly shaped particles. No rodlike morphology can be observed for (Ho → Lu, Y)PO_4 samples.

The morphology and structure of the products were further characterized by TEM and HRTEM. TEM and HRTEM images and the selected area electron diffraction (SAED) patterns of

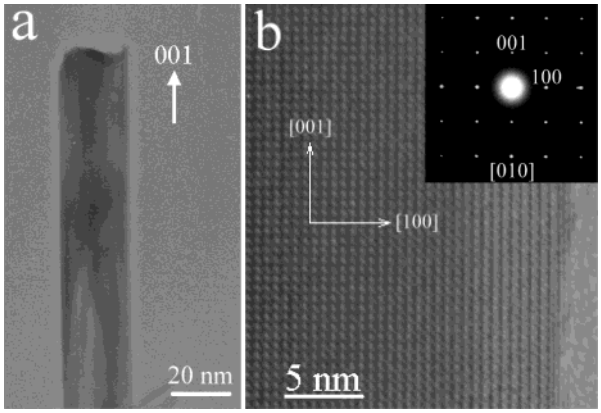

Figure 5. (a) TEM image of a single $CePO_4$ nanowire. (b) HRTEM image of a single nanowire with the clear lattice fringes of [001] with a spacing 0.652 nm and [100] with a spacing 0.608 nm. Inset in part b: the corresponding electron diffraction shows a single crystal recorded from the [010] zone axis.

$CePO_4$, $GdPO_4$, and $DyPO_4$ are presented in Figures 5, S4, and S5 (Figures S4 and S5, Supporting Information), respectively. Figures 5a, S4a, and S5a show the low magnification TEM images of the obtained $LnPO_4$ nanowires, further demonstrating that the obtained products have wirelike morphology. The HRTEM images (Figures 5b, S4b, and S5c) taken from a single nanowire show the clearly resolved planes of (001) and (100). The (001) planes are oriented parallel to the nanowire growth axis, indicating that the direction of nanowire growth is along the *c* axis. The SAED pattern (inset in Figures 5b, S4b, S5b) taken from a single nanowire can be indexed as a hexagonal $LnPO_4$ single crystal recorded from the [010] zone axis. The same results were also obtained for the six other $LnPO_4$ nanowires/nanorods. TEM observations for all wirelike samples show that each nanowire has a single crystal and that the growth direction of nine $LnPO_4$ nanowires/nanorods is the same, along the *c* axis, in good agreement with the XRD analyses. Energy-dispersive X-ray spectroscopy (EDS) analysis shows that the sample contains Ln, P, and O elements (Figure S6, Supporting Information). The composition of the products as extracted from the EDS analysis gives an Ln/P/O atomic ratio of ~1:1:4.2, in agreement with $LnPO_4$.

Figure S7 (Supporting Information) shows FTIR spectra of the obtained $LnPO_4$ (Ln = La → Dy) and (Ho → Lu, Y)PO_4 samples. Present FTIR data for lanthanide orthophosphates agree with reported values[46] and show the presence of a discrete PO_4 group; no pyrophosphate (P_2O_7 group, a typical band appearing at 1265−1267 cm^{-1}) impurity could be detected. There is a noticeable shift in the absorption frequencies depending on different lanthanide phosphates. For example, the absorption peak (615 or 951 cm^{-1} for $LaPO_4$) is systematically shifting into a higher frequency (626 or 985 cm^{-1} for $DyPO_4$) from $LaPO_4$ to $DyPO_4$, as clearly indicated in Figure S7. The systematic frequency shifts can be associated with the decrease in ionic radius from La^{3+} to Dy^{3+} (the effect of the lanthanide contraction).

The products obtained were further examined by XPS analysis. The XPS spectra of hexagonal $LaPO_4$ nanowires shown in Figure S8 (Supporting Information) give further evidence for the composition and purity of the products. All the peaks were calibrated by using C 1s (284.8 eV) as the reference. The binding energies of the XPS peaks are consistent with that reported for bulk $LaPO_4$.[40c,47] The peak at 133.8 eV (P 2p) suggests that phosphorus in the products exists as pentavalent oxidation states (P^{5+}).[48] The atomic ratio of La to P based on semiquantitative XPS analysis is about 1:1. The XPS data demonstrate that the product is pure $LaPO_4$, which agrees with the results of XRD and FTIR analyses. The XPS results for other lanthanide phosphates also illustrate that the products were completely formed in the stoichiometric ratio and that P exists in the P^{5+} state (data not shown here).

Controlled experiments were carried out to investigate the influence of pH and hydrothermal reaction temperature on the synthesis of $LnPO_4$ samples and the phase evolution. It is found that pH has some effect on the length and aspect ratio of the nanowires but little on the morphology of the nanowires. $LnPO_4$ (La → Dy) nanowires were always obtained at pH 1−7. Hexagonal $LnPO_4$ (Ce → Dy) nanowires were obtained at pH 1−7 by a hydrothermal process at 150 °C for 12 h. Increasing the pH of the precursor mixture resulted in an increase in the lengths and aspect ratios of the nanorods. As for $LaPO_4$, when the pH of the precursor suspension was increased to 4−5, the product after a hydrothermal treatment at 150 °C for 12 h had a monoclinic structure and wirelike morphology (data not shown). The reaction temperature can cause the phase evolution. When temperatrue was increased to 220 °C, monoclinic $LnPO_4$ (La → Tb) nanorods/nanowires were obtained at pH 1−7, and the obtained (Ho → Lu, Y)PO_4 nanoparticles have a tetragonal structure. Below pH 1, no precipitate was obtained. When the pH was increased over 7, the mixture of $LnPO_4$ and lanthanide hydroxides was obtained. Our results demonstrate that $LnPO_4$ (La → Dy) nanowires prepared at 150 °C for 12 h, pH 1−2 all have a hexagonal structure.

II. Structure Transition of $LnPO_4$ from Hexagonal to Monoclinic after Calcination. After all $LnPO_4$ samples obtained by hydrothermal treatment were calcined at 900 °C in air for 3 h, it was found that the hexagonal structure for $LnPO_4$ (La → Tb) nanowires/nanorods transforms into the monoclinic structure for corresponding materials. The hexagonal $DyPO_4$ is an exceptional case, and it converts to the tetragonal structure. Tetragonal (Ho → Lu, Y)PO_4 samples maintain their original structure after calcination. Moreover, the morphology of nanowires was not altered by calcination. Figure S9 (Supporting Information) shows XRD patterns of the obtained monoclinic $LnPO_4$ products by calcination, and from the figure it is clear that all the diffraction peaks for each sample could be indexed to a pure monoclinic phase [space group: $P2_1/n$ (14)] of (La → Tb)PO_4, in agreement with the reported data in the JCPDS cards. As for the hexagonal $DyPO_4$ sample, the tetragonal structure was obtained after calcination (Figure S10, bottom, Supporting Information). The XRD patterns of the calcined YPO_4 and $HoPO_4$ products are shown in Figure S10, and from the figure it is clearly seen that the tetragonal structure in the (Ho → Lu, Y)PO_4 samples remains unchanged (the calcined $ErPO_4$, $TmPO_4$, $YbPO_4$, and $LuPO_4$ smaples all have the tetragonal structure; data not shown here). TEM images of the

(46) Hezel, A.; Ross, S. D. *Spectrochim. Acta* **1966**, *22*, 1949.

(47) Jørgensen, S.; Horst, J. A.; Dyrlie, O.; Larring, Y.; Ræder, H.; Norby, T. *Surf. Interface Anal.* **2002**, *34*, 306 (XPS).

(48) (a) Splinter, S. J.; Rofagha, R.; Mcintyre, N. S.; Erb, U. *Surf. Interface Anal.* **1996**, *26*, 471. (b) Yu, J. C.; Zhang, L. Z.; Zheng. Z.; Zhao, J. C. *Chem. Mater.* **2003**, *15*, 2280.

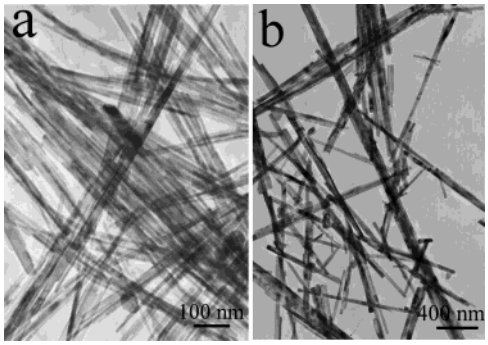

Figure 6. TEM images of monoclinic $LnPO_4$ nanowires/nanorods obtained by calcination of as-made corresponding products at 900 °C. (a) $LaPO_4$, (b) $CePO_4$.

obtained monoclinic $LaPO_4$, $CePO_4$, $PrPO_4$, and tetragonal $DyPO_4$ nanowires/nanorods are presented in Figures 6a, 6b, S11c, and S11d (Figure S11, Supporting Information), respectively. It is clearly shown that the morphologies of nanowires/nanorods have remained the same after calcination at high temperature, indicating that $LnPO_4$ nanowires/nanorods are very stable. With close examinations of each nanowire/nanorod by TEM, we found that the surfaces of nanowires/nanorods become coarser as compared to those of corresponding hexagonal materials, an effect which is believed to be caused by calcination.

It is worth noting that $DyPO_4$ is an exceptional case. According to previous studies,[30] it can crystallize in the hexagonal, monoclinic, or tetragonal form. In fact, all (La → Dy)PO_4 can only crystallize in a monoclinic structure when directly prepared by a solid-phase reaction at high temperature,[26a] while (Ho → Lu, Y)PO_4 have the tetragonal structure when prepared by the same method.[49] As compared with $LnPO_4$ prepared by a hydrothermal method, the same phenomena for crystal phase change can also be oberved for $LnPO_4$ obtained directly by high-temperature solid-phase synthesis. We have also prepared $DyPO_4$ crystals by a direct solid-phase reaction and found that only a monoclinic structure can be observed for $DyPO_4$. Why does the hexagonal structure for $DyPO_4$ nanowires obtained by the hydrothermal method convert to the tetragonal but not the monoclinic after calcination? Figure 1 shows that $DyPO_4$ exists in the boundary positions between the hexagonal and the tetragonal, which also indicates that $DyPO_4$ may crystallize in the tetragonal phase under certain conditions. Overall, $DyPO_4$ crystals can be obtained either in the tetragonal phase or in the monoclinic phase depending on the experimental conditions.

III. Absorption Spectra of $CePO_4$ Nanowires. Cerium compounds such as $CePO_4$, CeP_2O_7, and CeO_2 have been known to have strong absorption for the ultraviolet.[50] The optical absorption spectra of $CePO_4$ nanowires were measured and compared with those of bulk $CePO_4$. The absorption spectra of $CePO_4$ nanowires (red line) and bulk $CePO_4$ (blue line) are shown in Figure 7. The observed absorption peaks are caused by f−d electron transitions.[51] The absorption spectrum of $CePO_4$

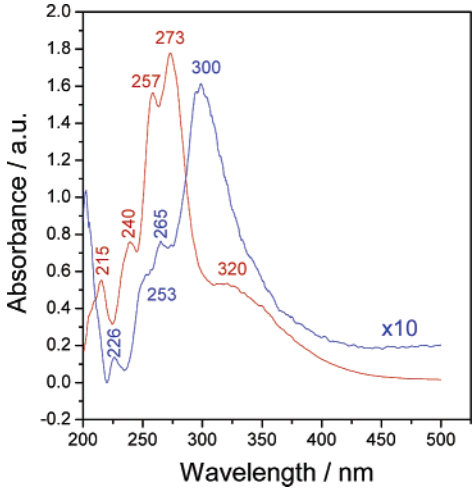

Figure 7. Absorption spectra of $CePO_4$ nanowires (red line) and bulk $CePO_4$ (blue line).

nanowires consists of five peaks with maxima at 215, 240, 257, 273, and 320 nm (Figure 7, red line), which correspond to the transitions from the ground state $^2F_{5/2}$ ($4f^1$) of Ce^{3+} to the five crystal field split levels of the Ce^{3+} $^2D(5d^1)$ excited states. It can be seen that the intensity of the peak at 273 nm is the strongest one. On the contrary, the absorption spectrum of bulk $CePO_4$ has four peaks with maxima appearing at 226, 253, 265, and 300 nm (Figure 7, blue line), in agreement with the reported values in the literature.[50a] The peak at 300 nm shows the strongest intensity, which is different from that of $CePO_4$ nanowires. Moreover, the broad peak at 320 nm for $CePO_4$ nanowires was not observed for bulk $CePO_4$, which may be attributable to the formation of low dimensional wirelike $CePO_4$. This differential spectral behavior observed for $CePO_4$ nanowires and bulk $CePO_4$ might be ascribed to the distorted lattices. It is generally considered that the degree of disorder in the nanomaterials is relatively high, thereby a lower crystal field symmetry might be induced in such materials.[52] The cell volume of $CePO_4$ nanowires calculated from the XRD pattern is 280.41 Å, while the cell volume of bulk $CePO_4$ is 267.32 Å. The increase in the cell volume of $CePO_4$ nanowires indicates that the lattices are more distorted in the nanowires than in the bulk and that the crystal field symmetry is lower in the former than in the latter.[52] Lower crystal field symmetry means that it is easy for the excited Ce^{3+} 5d degenerate states to be completely split into five energy levels, and thus five peaks in optical absorption spectra of $CePO_4$ nanowires can be observed (Figure 7, red line). The lattice deformation may contribute to the change of band structure in nanowires, thus giving rise to the absorption peak shifts as compared with bulk material.

IV. Rare Earth Doped Hexagonal $LnPO_4$ Nanowires Synthesis and Photoluminescence. Eu^{3+} doped $LaPO_4$ nanowires were prepared by the hydrothermal method, and in this work, the concentration of dopant Eu ions is 5 mol %, so this phosphor can be expressed as $La_{0.95}Eu_{0.05}PO_4$. Figure S12 (Supporting Information) shows a representative TEM image of the obtained $La_{0.95}Eu_{0.05}PO_4$ product, and from the figure it

(49) (a) Milligan, W. O.; Mullica, D. F.; Beall, G. W.; Boatner, L. A. *Inorg. Chim. Acta* **1982**, *60*, 39. (b) Milligan, W. O.; Mullica, D. F.; Beall, G. W.; Boatner, L. A. *Acta Crystallogr.* **1983**, C*39*, 23.
(50) (a) Imanaka, N.; Masui, T.; Itaya, M. *Chem. Lett.* **2003**, *32*, 400. (b) Imanaka, N.; Masui, T.; Hirai, H.; Adachi, G. Y. *Chem. Mater. 2003*, **2003**, *15*, 2289.
(51) Nakazawa, E.; Shiga, F. *Jpn. J. Appl. Phys.* **2003**, *42*, 1642.
(52) (a) Wei, Z.; Sun, L.; Liao, C.; Yin, J.; Jiang, X.; Yan, C. *J. Phys. Chem. B* **2002**, *106*, 10610. (b) Tao, Y.; Zhao, G.; Zhang, W.; Xia, S. *Mater. Res. Bull.* **1997**, *32*, 501. (c) Tissue, B. M. *Chem. Mater.* **1998**, *10*, 2837. (d) Williams, D. K.; Bihari, B.; Tissue, B. M.; McHale, J. M. *J. Phys. Chem. B* **1998**, *102*, 916.

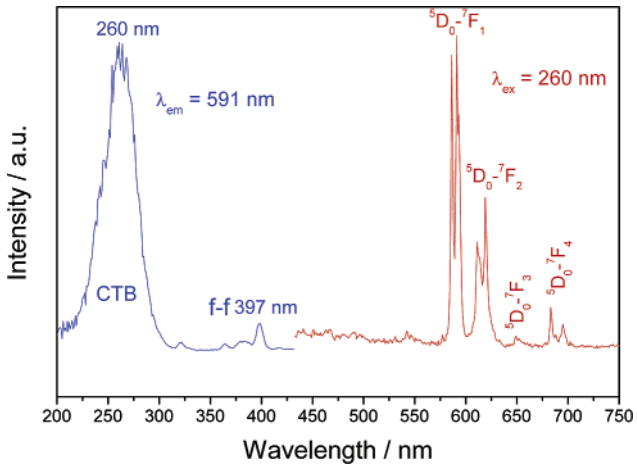

Figure 8. Excitation (blue line) and emission (red line) spectra of as-prepared $La_{0.95}Eu_{0.05}PO_4$ nanowires.

can be seen that the sample consists almost entirely of nanowires/nanorods with diameters of 5−30 nm and lengths of several micrometers.

The excitation spectrum obtained by monitoring the emission of $LaPO_4$/Eu nanowires is shown in Figure 8 (blue line). The broad band with a maximum at 260 nm shown in the spectrum originates from the excitation of the oxygen-to-europium charge-transfer band (CTB). By comparison with that of bulk $LaPO_4$/Eu (253 nm),[53] a small shift of the CT band could be observed for $LaPO_4$/Eu nanowires (260 nm). As reported by previous studies,[52a,54] the peak position of the CT band is involved in the length of Eu−O bond; the longer the Eu−O bond is, the longer the wavelength of the CT band position will be. In this study, we have already pointed out that a relatively larger cell volume can be observed for $LaPO_4$/Eu nanowires compared to bulk $LaPO_4$/Eu. This indicates that the average Eu−O bond distance is relatively longer in $LaPO_4$/Eu nanowires, and as a consequence, a small redshift of the CT band would be observed. The general f−f transitions within the Eu^{3+} $4f^6$ electron configuration in the longer wavelength region (300−500 nm) can also be observed (Figure 8, blue line). These peaks correspond to the direct excitation of the Eu^{3+} ground state into higher levels of the 4f-manifold such as $^7F_0-^5L_6$ at 397 nm. Upon excitation into the CTB of Eu^{3+} at 260 nm, the emission spectrum of powders of hydrothermally prepared $LaPO_4$/Eu nanowires (Figure 8, red line) consists of sharp lines as expected for the transitions between europium levels, which couple only very weakly to lattice phonons. Among $^5D_0-^7F_J$ ($J = 1, 2, 3, 4$) emission lines of Eu^{3+} shown in Figure 8 (red line), the magnetic-dipole transition $^5D_0-^7F_1$ (591 nm) is the most prominent group, which is characterized by orange-red emission. Emission from the higher energy levels ($^5D_1$, $^5D_2$) of Eu^{3+} is not detected due to multiphoton relaxation based on the vibration of phosphate groups (ca. 1067 cm^{-1}), which can bridge the gaps between the higher energy levels ($^5D_1$, $^5D_2$) and the lowest $^5D_0$ level of Eu^{3+} effectively. The intensity of transitions between different J-number levels depends on the symmetry of the local environment of the europium ions and can be described in terms of the Judd−Ofelt theory.[55] The splitting observed in each group of luminescence lines (Figure 8, red line) is caused by the crystal field. The above luminescent properties of Eu^{3+} in the crystalline $LaPO_4$ nanowires are basically in agreement with those for bulk $LaPO_4$/Eu reported previously, indicating that Eu^{3+} ions have been successfully doped into host $LaPO_4$ nanowires. The transition ($^5D_0-^7F_1$) displays more intensity than that of the transition ($^5D_0-^7F_2$) due to localized energy transfer.

Although the transition energies are the same for nanowires and bulk particles, the intensity patterns of their luminescence spectra show small differences. Comparing bulk $LaPO_4$/Eu[52a] and $LaPO_4$/Eu nanowires, we find that the intensities of the lines belonging to the $^5D_0-^7F_4$ are different in the two cases. A similar difference can be observed for the components of the $^5D_0-^7F_2$ transition. The intensity of the luminescence lines of $LaPO_4$/Eu and other lanthanide doped phosphates is known to depend on the orientation of the unique crystal axis relative to the polarization vector of the incident light.[56] Since our excitation light was partly polarized, any preferred orientation of the nanowires in the powders will influence the intensity pattern of the emission spectra. Meanwhile, the ratio of the intensity of $^5D_0-^7F_1$ to $^5D_0-^7F_2$ for $LaPO_4$/Eu nanowires is smaller than that of bulk $LaPO_4$/Eu. Considering that the $^5D_0-^7F_2$ transition is hypersensitive to the symmetry of the crystal field, and it will be relatively strong if the symmetry of the crystal field is relatively low. By comparison with bulk $LaPO_4$/Eu, the increase of the intensity of the $^5D_0-^7F_2$ transition for nanowires is obviously correlated with the distorted lattices. The above results have demonstrated that the lattices are more distorted in the $LaPO_4$/Eu nanowires than in the corresponding bulk material.

In contrast to semiconductors such as CdSe, CdTe, and ZnO nanocrystals showing unique absorption and fluorescence characteristics due to quantum size effects,[57] the fluorescence of the $LaPO_4$/Eu nanowires originates from their bulk properties (i.e., transitions between d and f electron states and their local symmetry). In fact, particle size effects on the luminescence of $LaPO_4$/Eu nanowires are expected to be weak, since transitions of the well-shielded f electrons are mainly affected by the local symmetry of the crystal site.

V. Crystal Structure of $LnPO_4$ and the Possible Growth Mechanism of Hexagonal $LnPO_4$ Nanowires. In general, three kinds of mechanisms including vapor−liquid−solid (VLS) growth,[58] solution−liquid−solid (SLS) growth,[59] and template-mediated processes[60] have been proposed for the formation of crystalline nanowires. Clearly, the formation of the nanowires in our synthetic system would not be dominated by the above-mentioned three processes. To date, the shape of metal nanoparticles or semiconductor nanocrystals has mainly been controlled by the presence of surfactants, polymers or strong

(53) Yu, M.; Lin, J.; Fu, J.; Zhang, H. J.; Han, Y. C. *J. Mater. Chem.* **2003**, *13*, 1413.
(54) (a) Hoefdraad, H. E. *J. Solid State Chem.* **1975**, *15*, 175. (b) Tao, Y.; Zhao, G.; Ju, X.; Shao, X.; Zhang, W.; Xia, S. *Mater. Lett.* **1996**, *28*, 17.
(55) (a) Judd, B. R. *Phys. Rev.* **1962**, *127*, 750. (b) Ofelt, G. S. *J. Chem. Phys.* **1962**, *37*, 511.
(56) Meyssamy, H.; Riwotzki, K.; Kornowski, A.; Naused, S.; Haase, M. *Adv. Mater.* **1999**, *11*, 840.
(57) (a) Peng, X.; Manna, L.; Yang, W.; Wickham, J.; Scher, E.; Kadavanich, A.; Alivisatos, A. P. *Nature* **2000**, *404*, 59. (b) Peng, Z. A.; Peng, X. G. *J. Am. Chem. Soc.* **2001**, *123*, 183. (c) Tang, Z.; Kotov, N. A.; Giersig, M. *Science* **2002**, *297*, 237. (d) Guo, L.; Ji, Y.; Xu, H.; Simon, P.; Wu, Z. *J. Am. Chem. Soc.* **2002**, *124*, 14864.
(58) Morales, A. M.; Lieber, C. M. *Science* **1998**, *279*, 208.
(59) Trentler, T. J.; Hickman, K. M.; Goel, S. C.; Viano, A. M.; Gibbons, P. C.; Buhro, W. E. *Science* **1995**, *270*, 1791.
(60) Harada, M.; Adachi, M. *Adv. Mater.* **2000**, *12*, 839. (b) Li, Y.; Li, X.; Deng, Z.; Zhou, B.; Fan, S.; Wang, J.; Sun, X. *Angew. Chem., Int. Ed.* **2002**, *41*, 33.

chelating ligands. Peng et al. presented a three-stage shape evolution mechanism based on the spherical diffusion controlled crystal growth theory, which elucidated the shape evolution of CdSe nanocrystals well.[61] However, this theory has seldom been used to explain the formation mechanism of 1D nanowires/nanorods in surfactant-free systems. Yu et al. have recently reported the general synthesis of metal tungstate nanorods by the hydrothermal process and found that the formation process of the nanorods could fit the spherical diffusion model well.[62] In our system, the formation of the nanowires could also be explained by this theory. Here, the strong pH-dependent relation with the lengths and aspect ratios of the nanowires is due to the sensitive influence of the pH on the solute concentrations ($[Ln^{3+}]$ and $[PO_4^{3-}]$). This observation suggests that the 1D growth stage was rightly captured by maintaining the solute concentrations in the correct range, through control of the pH. The obvious 1D growth stage observed here is also in agreement with the previous model proposed by Peng et al.[61]

$LnPO_4$ (Ln = La → Dy) nanowires that were fabricated have a hexagonal crystal structure, similar to that of ZnO[63] and $Ln(OH)_3$,[25] which are well-known to exhibit anisotropic growth. Studying on the natural chemical character of lanthanide phosphates can help us to understand the growth mechanism of lanthanide phosphate nanowires. In this solution phase process, the morphology of the final product is largely determined by the anisotropic nature of the building blocks, that is, the 1D characteristics of the infinite linear chains of hexagonal structured $LnPO_4$ (Ln = La → Dy) in the crystalline phase. The crystal structure of representative hexagonal $CePO_4$ is shown in Figure 9.[64] Each cerous ion is coordinated to eight oxygen atoms, four at distances of 2.34 Å and four at 2.66 Å. The shorter distances are to the corners of four different tetrahedra, linking atoms which are practically coplanar. The longer distances extend to pairs of oxygens forming the edges of two tetrahedra, one above and one below the plane of the four shorter distances. A given phosphate group is coordinated to six cerous ions, each corner by one short bonding distance, and opposite edges by longer bonding distances. The cerium−cerium separation is 4.13 Å. The phosphate ion has been taken to be a tetrahedral grouping of oxygens about phosphorus, with the P−O distance fixed at 1.56 Å (Figure 9a). The overall structure of this compound may be described as columns built up of alternate cerous and phosphate ions, extending along the *c* axis, each column linked to four neighboring columns is such that open channels run though the structure along the hexagonal axis (Figure 9b). The packing structure of hexagonal $CePO_4$ viewing along the *a* axis can be described as infinite linear chains, parallel to the *c* axis (Figure 9b). From a structural point of view, hexagonal $CePO_4$ consists of infinite linear chains extending along the *c* axis. From a thermodynamic perspective, the activation energy for the *c* axis direction of growth of hexagonal $LnPO_4$ is lower than that of growth perpendicular to the *c* axis.[65] This means a higher growth rate along the *c* axis and a lower one perpendicular to the *c* axis to form $LnPO_4$ nanowires/nanorods that grow preferentially along the [001] direction. This is in very good agreement with the abnormally strong intensity of the (200) peak in the XRD patterns (Figure S1, Supporting Information) and HRTEM results (Figures 5, S4, and S5). Hexagonal $LnPO_4$ (Ln = La, Pr, Nd, Sm, Eu, Gd, Tb, and Dy) are isostructural with hexagonal $CePO_4$; therefore, the formation of other $LnPO_4$ nanowires/nanorods can also be explained based on its highly anisotropic character along the *c* axis, in agreement with HRTEM observation (Figures 5, S4, and S5). It is this structural feature that plays a key role in the highly intrinsic preferential growth along the *c* axis of $LnPO_4$ (Ln = La → Dy) nanowires.

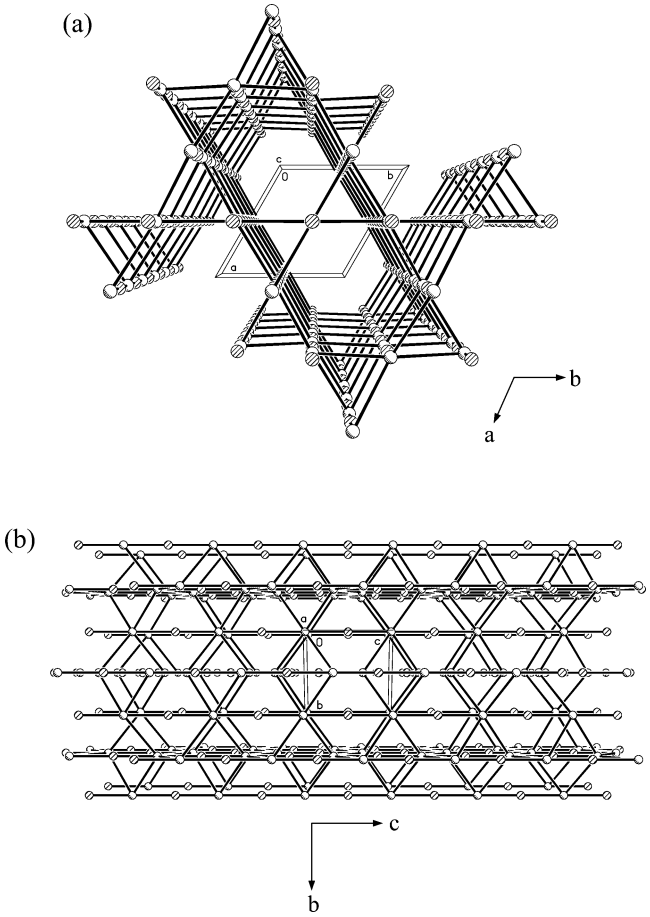

Figure 9. (a) Packing view of $CePO_4$ along the *c* axis. Each column is linked to four neighboring columns; open channels run though the structure along the hexagonal axis (the *c* axis). Oxygen atoms are omitted for clarity. (b) Packing view of $CePO_4$ along the *a* axis. Each column is built up of alternate cerous (shadow circles) and phosphate ions (open circles) and extends along the *c* axis. Oxygen atoms are omitted for clarity.

On the contrary, tetragonal (Ho → Lu, Y)PO_4 has no preferred growth direction in the crystalline phase based on their crystal structure.[49] The molecular arrangements of tetragonal $LuPO_4$ viewing along the *a*, *b*, and *c* axis are presented in Figure 10a, b, and c, respectively. Compound $LuPO_4$ crystallizes in the tetragonal system conforming to space group $I4_1/amd$. The Lu atom is eight-coordinated to oxygen atoms with two unique metal−oxygen bond distances. Each of these discrete lengths are tetrahedrally oriented orthogonal to one another thus forming a distorted dodecahedron, which is a bisphenoid contains two interpenetrating distorted tetrahedra distinguished by the bond lengths Lu−O's = 2.262 Å and Lu−O's = 2.344 Å. In other words, the eight vertexes of the dodecahedron are not equivalent

(61) (a) Peng, Z. A.; Peng, X. G. *J. Am. Chem. Soc.* **2001**, *123*, 1389. (b) Peng, Z. A.; Peng, X. G. *J. Am. Chem. Soc.* **2002**, *124*, 3343.
(62) Yu, S. H.; Liu, B.; Mo, M. S.; Huang, J. H.; Liu, X. M.; Qian, Y. T. *Adv. Funct. Mater.* **2003**, *13*, 639.
(63) Huang, M.; Mao, S.; Feick, H.; Yan, H.; Wu, Y.; Kind, H.; Weber, E.; Russo, R.; Yang, P. *Science* **2001**, *292*, 1897.
(64) Mooney, R. C. L. *Acta Crystallogr.* **1950**, *3*, 337.
(65) Murphy, K. E.; Altman, M. B.; Wunderlich, B. *J. Appl. Phys.* **1977**, *48*, 4122.

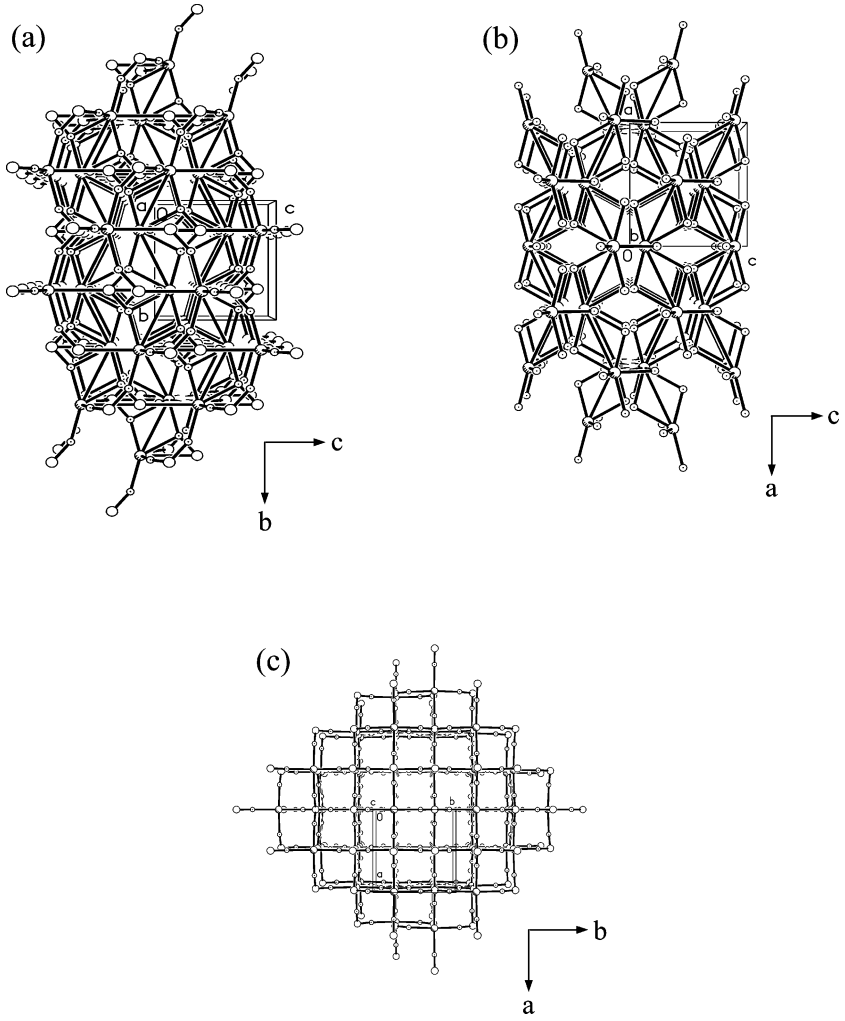

Figure 10. (a) Perspective view along the *a* axis of the molecular packing of $LuPO_4$. (b) Perspective view along the *b* axis of the molecular packing of $LuPO_4$. (c) Perspective view along the *c* axis of the molecular packing of $LuPO_4$.

but are divided into two bisphenoidal sets, and those within each set are equal. The phosphate group PO_4 is a distorted tetrahedron with variable bond angles. No anisotropic nature can be observed in the tetragonal structured $LuPO_4$, which is different from hexagonal structured $CePO_4$. Therefore, the prepared $LuPO_4$ sample presents particle morphology instead of nanowires. Tetragonal $HoPO_4$, $ErPO_4$, $TmPO_4$, $YbPO_4$, and YPO_4 are isostructural with tetragonal $LuPO_4$;[49] therefore, the resulting irregularly shaped particle morphology can also be explained based on their crystal structure.

Conclusions

This article describes the development of a simple hydrothermal process for the systematic preparation of $LnPO_4$ crystals that have been preformed by a facile hydrothermal process. It has been found that lanthanide phosphates $LnPO_4$ crystallize with hexagonal or tetragonal structure depending on the ionic radius of the lanthanide ions. $LnPO_4$ (Ln = La → Dy) nanowires/nanorods crystallize in the hexagonal form, while (Ho → Lu, Y)$LnPO_4$ materials exist in the hexagonal structure under low-temperature hydrothermal conditions. The obtained hexagonal $LnPO_4$ (Ln = La, Ce, Pr, Nd, Sm, Eu, Gd, Tb, and Dy) products have wirelike morphology. On the contrary, tetragonal $LnPO_4$ (Ln = Ho, Er, Tm, Yb, Lu, Y) samples prepared under the same experimental conditions consist of irregularly shaped particles. The structure transition of $LnPO_4$ (Ln = La → Tb) nanowires/nanorods from the hexagonal to the monoclinic monazite can be observed, while their morphology is retained after calcination at 900 °C in air. In the case of hexagonal $DyPO_4$ nanowires, they are transformed to tetragonal $DyPO_4$ nanowires by calcination. No phase change can be observed for the tetragonal structured (Ho→ Lu, Y)PO_4 after calcination. The as-synthesized $LnPO_4$ (Ln = La → Dy) products consist almost entirely of nanowires/nanorods with diameters of 5−120 nm and lengths ranging from several hundreds of nanometers to several micrometers. Europium doped $LaPO_4$ nanowires were also successfully prepared. The absorption spectra of $CePO_4$ nanowires and photoluminescent properties of $LaPO_4$/Eu nanowires were reported. Based on the crystal structure of $LnPO_4$, we suggest that the growth of $LnPO_4$ (Ln = La → Dy) nanowires is determined by its highly anisotropic character along the *c* axis. The simplicity of the hydrothermal process, cheapness, and availability of raw materials, without the need for catalysts or templates, are important considerations for industrial manufacturing. Lanthanide phosphate nanowires could be doped with different lanthanide elements and used for fluorescent lamps, new type plasma display panels excited by ultraviolet radiation, and luminescent labels for biomolecules. We believe that other $LnPO_4$ phosphors with a wirelike morphology such

as $LaPO_4$/Tb, $LaPO_4$/Ce/Tb, and (La, Gd)PO_4/Tb can be prepared by the same method. Metal phosphates, also known as a component of bones and teeth, have proven to be inert and safe, with no known side effects to the human body. The features of lanthanide doped lanthanide phosphates are their high quantum yield, their high chemical stability, and their expected low toxicity, making them particularly suitable for biological labeling applications based on the individual rare earth doped $LnPO_4$ nanowire.

Acknowledgment. This work was supported by the National Natural Science Fund of China and the Guangdong Province "The Tenth Five-Year Plan" Key Projects (2001A1070103).

Supporting Information Available: XRD patterns; TEM and SEM images; EDS spectrum; FTIR spectra; XPS spectra (PDF). This material is available free of charge via the Internet at http://pubs.acs.org.

JA037280D